Two-dimensional electronic spectroscopy of a minimal Photosystem I complex reveals the rate of primary charge separation

Parveen Akhtar[†,‡,¶], Ido Caspy[§], Paweł J. Nowakowski[†], Tirupathi Malavath[§,‖], Nathan Nelson[§], Howe-Siang Tan[†,*], Petar H. Lambrev[‡,*]

[†] School of Physical and Mathematical Sciences, Nanyang Technological University, Nanyang Link 21, Singapore

[‡] Biological Research Centre, Szeged, Temesvári krt. 62, Szeged 6726, Hungary

[§] Department of Biochemistry and Molecular Biology, The George S. Wise Faculty of Life Sciences, Tel Aviv University, Tel Aviv 69978, Israel

[¶] ELI-ALPS, ELI-HU Non-profit Ltd., Wolfgang Sandner u. 3, Szeged 6728, Hungary

Abstract

Photosystem I (PSI), found in all oxygenic photosynthetic organisms, uses solar energy to drive electron transport with nearly 100% quantum efficiency, thanks to fast energy transfer among antenna chlorophylls and charge separation in the reaction center. There is no complete consensus regarding the kinetics of the elementary steps involved in the overall trapping, especially the rate of primary charge separation. In this work we employed two-dimensional coherent electronic spectroscopy to follow the dynamics of energy and electron transfer in a monomeric PSI complex from *Synechocystis* PCC 6803, containing only subunits A–E, K and M, at 77 K. We also determined the structure of the complex to 4.3 Å resolution by cryoelectron microscopy with refinements to 2.5 Å. We applied structure-based modelling using a combined Redfield-Förster theory to compute the excitation dynamics. The absorptive 2D electronic spectra revealed fast excitonic/vibronic relaxation on timescales of 50–100 fs from the high-energy side of the absorption spectrum. Antenna excitations were funneled within 1 ps to a small pool of chlorophylls absorbing around 687 nm, thereafter decaying with 4–20 ps lifetimes, independently of excitation wavelength. Redfield-Förster energy transfer computations showed that the kinetics is limited by transfer from these red-shifted pigments. The rate of primary charge separation, upon direct excitation of the reaction center, was determined to be 1.2–1.5 ps^{-1}. This result implies activationless electron transfer in PSI.

Introduction

Photosystem I (PSI) is found in all organisms capable of oxygenic photosynthesis, including cyanobacteria, eukaryotic algae and plants. The composition and structural organization of the multisubunit pigment-protein complex is highly conserved.[1-3] PSI of cyanobacteria is composed of 11–14 protein subunits,[4-6] 94–96 chlorophyll (Chl) *a* molecules and 22–24 carotenoids. Most antenna Chls and the six Chls of the reaction center (RC) are bound to the PsaA-PsaB heterodimer. Antenna Chls have overlapping absorption in the wavelength range 660–690 nm but long-wavelength Chl forms – "red Chls", absorbing at wave-

lengths longer than 700 nm are found in PSI from most organisms.[7-8]. The principal excitation trapping time at room temperature (RT) is 20–25 ps in PSI from the cyanobacterium *Synechocystis* PCC 6803.[9-11] This includes different processes of excitation migration in the antenna, transfer to the RC and electron-transfer steps leading to reduction of the phylloquinone acceptors A_1 and the formation of the stable radical pair $P_{700}^+A_1^-$. These individual processes are extremely difficult to disentangle experimentally. The tight packing of antenna Chls suggests ultrafast excitation energy transfer (EET); accordingly, equilibration components in the range of 0.2–0.6 ps are experimentally resolved.[12-13] The trapping time is independent of excitation wavelength indicating that exciton equilibration in the antenna is significantly faster and trapping occurs from a quasiequilibrated state.[13-14] A trap-limited model has been put forward, according to which excitations can visit the RC several times before charge separation (CS).[9, 15-17] On the other hand, the relatively long distances between the nearest antenna Chls and the RC encourage an alternative view of transfer-to-trap limited kinetics where CS is fast and virtually irreversible.[8, 11, 18]

Several groups have attempted to determine the *intrinsic* CS rate theoretically or experimentally and proposed values in the range of $(0.5–3\ ps)^{-1}$.[11, 19-21] An experimentally observed lifetime of 2–4 ps is ascribed to energy equilibration between the bulk antenna Chls and the red forms by most authors.[8, 10-11, 22-23] However, in studies on PSI from *C. reinhardtii* which does not contain Chls absorbing above 700 nm, the spectral changes on this timescale were interpreted as arising from excitation of the RC pigments followed by CS.[17, 21, 24] A similar interpretation was proposed for the plant PSI core.[25-27] Conversely, ultrafast CS on a timescale as short as 100 fs has been detected upon excitation on the red absorption edge and interpreted as the result of quantum mixing of exciton and charge-transfer states in the RC.[28-29] Thus, at present there is no general consensus on the kinetics of the important phases of energy and electron transfer in PSI.

The high quantum yield of CS is still observed upon excitation of the PSI core antenna even at very low temperatures[30] and reversible photochemistry happens in about half of the RCs.[31] At cryogenic temperatures, as uphill transfer is blocked, the red Chls become deep excitation traps competing with the RC.[30] Photochemical trapping occurs in 10–50 ps, presumably limited by slow EET,[32] whereas the red Chls decay over hundreds of ps to ns.[32-33] The red Chls are populated on a timescale of 4–6 ps at low temperature[32, 34-35] – slightly slower than at RT. A general slowing down of EET rates is expected[36] and experimentally verified in different photosynthetic complexes.[37-38] Besides that, the CS dynamics at low temperature is not well understood.

In the past decade, two-dimensional electronic spectroscopy (2DES) has proved itself as one of the most powerful tools to study the excitation dynamics in photosynthetic complexes.[39-40] The main advantages of 2DES lie in its ability to resolve the dynamics on both excitation and detection wavelength with the highest possible time resolution offered by broadband excitation pulses. In practice, reaching this potential for large multichromophore complexes has proved technically difficult because they require very low excitation powers, to avoid multiphoton effects, combined with high dynamic range, necessary to resolve many overlapping kinetic and spectral components. 2DES has been especially useful to uncover the role of quantum coherence, appearing as temporal oscillations of peak amplitudes in the 2D spectra, in light harvesting and CS.[41-43]

Previously, 2DES was performed at RT on PSI complexes from plants[26] and cyanobacteria [44-45] with results interpreted in the frame of existing models. To gain further insight into the dynamics of energy and electron transfer, we performed 2DES experiments on monomeric PSI from *Synechocystis* PCC 6803 ΔFIJL mutant strain at RT and 77 K. This "minimal" PSI complex contains only the subunits A-E, K and M but retains the overall trapping kinetics of the trimeric PSI from *Synechocystis* PCC 6803.[33] Compared to the WT PSI, the minimal complex contains fewer Chls (88) and significantly reduced absorption in the wavelength range 695–705 nm (Supplementary Figure S1), facilitating selective excitation of antenna and RC Chl pools. Taking advantage of the combined time resolution and spectral selectivity of 2DES, we resolve ultrafast sub-100-fs spectral equilibration upon excitation of antenna Chls and a 0.6–0.8 ps primary CS upon direct excitation of the RC. The experimental results are supported by structure-based theoretical modelling.

Experimental methods

Sample preparation and handling

Subunit-depleted PSI was isolated from *Synechocystis* PCC 6803 mutant lacking the PSI subunits PsaF, PsaI, PsaJ, PsaL (ΔFIJL), deleting the PsaJ-PsaF operon from a ΔPsaL strain.[5] PSI was isolated, purified and crystallized as described by Malavath et al.[6] Crystals were dissolved by incubation (while gently agitating) in a buffer medium containing 0.03 % dodecyl-β-maltoside (β-DDM) before measurements.

Absorption spectra in the range of 350–750 nm were recorded at RT with a Thermo Evolution 500 dual-beam spectrophotometer. The samples were diluted in 20 mM Tricine buffer (pH 7.8) with 0.03% β-DDM to an absorbance of one at the red maximum. The measurements were performed in a standard glass cell of 1-cm optical path length with 1 nm spectral bandwidth.

For 2DES experiments at RT, a protocol described previously was followed.[26] Briefly, the samples were suspended in degassed buffer (pH 7.8) to absorbance of 0.3 at the Chl *a* Q_y band (680 nm) in a 1-mm optical pathlength. Additionally, 20 mM sodium ascorbate and 40 μM phenazine methosulfate was added to the suspension to ensure rapid re-reduction of the RC. The samples were continuously circulated during the measurement. For 77 K measurements, the buffer medium was supplemented with 60% (v/v) glycerol, 20 mM sodium ascorbate and 40 μM phenazine methosulfate. Absorbance was adjusted to 0.3 at 680 nm; the sample was placed between sapphire windows separated with a 0.5-mm thick Teflon spacer and cooled in a vacuum cryostat (Janis) with low-dispersion BaF_2 windows.

2D electronic spectroscopy

Fourier-transform femtosecond 2DES was performed at RT and 77 K using a partially collinear "pump-probe" geometry experimental setup producing absorptive 2D spectra.[46] Briefly, excitation pulses of ~30 fs are obtained by passing the output of an amplified Ti:sapphire laser system (Legend, Coherent) through a non-collinear parametric amplifier (TOPAS, Light Conversion). The excitation pulses are centred at 680 nm to coincide with the Chl *a* Q_y absorption band of PSI (Supplementary Figure S2). Pulse pairs with controllable inter-pulse delay time and phase difference are generated with an acousto-optic programmable dispersive filter (AOPDF) pulse shaper (Dazzler, Fastlite) that is also used as a secondary compressor to pre-compensate for dispersion. A white-light supercontinuum pulse generated in a 2-mm sapphire window is used as the third interaction pulse (probe/detection) after compressing with chirp mirrors. The probe polarization was 54.7° with respect to the pump. The probe beam was modulated (to subtract scattered pump light), split into signal (overlapped with the pump) and reference and measured with a spectrometer resolving the signal in detection wavelength (λ_t). The cross-correlation width of the excitation and probe pulses was ~40 fs (FWHM), determined by measuring the optical Kerr effect.

To avoid exciton annihilation and the build-up of photoproducts, the experiments were done with excitation pulses of very low energy – 1–1.5 nJ, equivalent to $\sim 5\times10^{12}$ photons/cm^2/pulse, to obtain maximal transient absorption signal of 2 mOD, or excitation probability of <0.01 PSI/pulse.

The time delay τ between the two excitation pulses was scanned between 0 and 150 fs in 3-fs steps for RT measurements and typically 0–300 fs in 5-fs steps for 77 K measurements applying a 2-phase cycling scheme ($\varphi = 0; \pi$) in a rotating frame of reference.[47] The signals (2D interferograms) were Fourier-transformed along τ to obtain 2D electronic spectra in the frequency/wavelength domain (with excitation/detection wavelengths λ_τ/λ_t). The nominal spectral resolution along the excitation wavelength was <3 nm (~50 cm^{-1}). The waiting time (T_w) between the excitation and probe pulses was scanned in 200 steps from −100 fs to 100 ps in a quasilogarithmic progression. For every $\tau/\varphi/T_w$ combination approx. 400 laser shots were collected, and the entire measurement cycle was repeated 10 times while monitoring the probe, reference, scattered pump, and pump-probe signals on a shot-to-shot basis. Subsequent cycles were compared with each other to ensure that no sample

degradation had taken place during the experiment. Finally, data averaging was done with outlier rejection using MAD (median absolute deviation to the median) algorithm with cut-off σ = 2.5. All data processing was done in MATLAB.

Cryo-EM structure determination

Roughly 50 large PSI crystals of the ΔFIJL mutant were collected using 0.7–1.0 mm Cryoloop (Hampton research) and released into a 0.5 ml Eppendorf tube containing 0.4 ml solution of 20 mM Tris (pH8) and 20% PEG 400. Following centrifugation at 14,000 rpm for 1 min, the supernatant was carefully removed, and the crystals were solubilized in 60 µl of a solution containing 20 mM MES-Tris (pH7) and 0.05% α-DDM at a Chl concentration of 5 to 7 mg/ml. The concentrated PSI was diluted to give final concentration of 3 mg Chl/ml. The resulting PSI solution (3 µl) was applied on glow-discharged holey carbon grids (Cu Quantifoil R1.2/1.3), before using a Vitrobot FEI (3 s blot at 4°C and 100% humidity). The images were collected using a 300 kV FEI Titan Krios electron microscope, with a slit width of 20 eV on a GIF-Quantum energy filter and Volta Phase Plate (Diamond Light Source). A Gatan K3-Summit detector was used in counting mode at a magnification of 165,000× (yielding a pixel size of 0.8328 Å), with a total dose of 43.485 $e^{-}Å^{-2}$. EPU was used to collect a total of 2,493 images, which were dose-fractionated into 40 video frames, with defocus values ranging from 0.9 µm to 3.0 µm, with increments of 0.3 µm. The collected micrographs were motion-corrected and dose-weighted using MotionCor2.[48] The contrast transfer function parameters were estimated using CtfFind 4.1.[48] A total of 286,538 particles were picked using reference-free picking in RELION v.3.[49] The picked particles were processed for reference-free 2D averaging and initial model building. Following 3D classification creation, a subset of 74,303 particles were pooled together and processed for 3D homogeneous refinement and post-processing using RELION. The reported resolutions were based on a gold-standard refinement, applying the 0.143 criterion on the FSC between the reconstructed half-maps (Supplementary Figure S3). The cryo-EM map is deposited to the Electron Microscopy Data Bank (EMD-12697).

To generate the ΔFIJL PSI, the crystal structure of *Synechocystis* PSI trimer model PDB 5OY0 [6] was selected. This model was manually fitted onto the cryo-EM density map rebuilt using Coot.[50] Stereochemical refinement was performed using phenix.real_space_refine in the PHENIX suite.[51] The final model was validated using MolProbity.[52] The refinement statistics are provided in Supplementary Table S1. Local resolution was determined using ResMap,[53] and the figures were generated using UCSF ChimeraX.[54] Structural data were deposited to the Protein Data Bank (ID 7O1V).

Structure-based modelling

Theoretical structure-based modelling of the kinetics of EET in the minimal PSI complex was performed applying a combined modified-Redfield–generalized-Förster theory, using the formalism described by Raszewski and Renger.[55] Details of the calculations of optical spectra and dynamics are given in Supplementary Information. The atom coordinates of the 88 Chls in the minimal PSI were taken from the cryo-EM structure. Transition dipole moment vectors were assumed along the N_B–N_D atoms and point-dipole approximation was used to calculate the exciton couplings, e.g. as in Byrdin et al.[56] We have not attempted to calculate the Chl site energies from the structure but used the energies obtained from INDO calculations on the DFT-optimized structure of PSI from *T. elongatus*.[57] The values for the six RC Chls were taken from Renger & Schlodder.[58] The site energies were then refined to fit the absorption spectrum of the minimal PSI. These optimized values may not accurately describe the real system; however, the qualitative features of the model discussed here have been confirmed to persist with different sets of site energies. The Frenkel exciton Hamiltonian, constructed using the Chl site energies and exciton couplings, was partitioned into exciton domains with a cutoff coupling energy V_c = 70 cm^{-1}. The largest exciton domain encompasses the six RC Chls; all other domains consist of 2–4 Chls (Supplementary Table S2). Exciton delocalization is only allowed between Chls in the same exciton domain. Exciton relaxation rates within the domains were calculated using modified Redfield theory, using an analytical expression for the spectral density of electron-vibrational coupling as in,[59] assuming Huang-Rhys factors S = 0.6 for the bulk antenna Chls, 1.8 for ecA_1-ecB_1 and 2 for the red Chls B32 and B37. Optical lineshapes were obtained from

non-Markovian POP-theory within secular approximation and Markov approximation for the off-diagonal electron-vibrational coupling. The rates of exciton transfer between excited states belonging to different domains are calculated using generalized Förster theory.[60-62] The exciton population dynamics was calculated using a master equation approach and the steady-state and time-dependent spectra were simulated after Monte-Carlo sampling of 2000 diagonal disorder realizations with an inhomogeneous width of 60–80 cm^{-1} and 140 cm^{-1} for the red Chls.

Results and discussion

Understanding 2D electronic spectra

The absorptive 2D electronic spectrum recorded at waiting time T_w is a map correlating two frequencies or wavelengths – excitation (λ_τ) and detection (λ_t). As the projection-slice theorem holds, the spectrum integrated over excitation frequency is identical to a conventional pump-probe transient absorption spectrum recorded at delay time T_w with broadband excitation pulses. Conversely, the 2D spectra can be thought of as transient absorption spectra spread over a range of excitation wavelengths. Selected 2D electronic spectra of PSI at different T_w are plotted in Figure 1A. To a first approximation, negative signals at (λ_τ, λ_t) can be interpreted as representing the population (ground-state bleaching) of excited states absorbing at λ_t after initial excitation of states absorbing at λ_τ. Thus, cross-peaks in the 2D spectra generally indicate EET $\lambda_\tau \rightarrow \lambda_t$. Assuming first-order EET kinetics, we obtain the relevant timescales by global multiexponential analysis of the data [63]. The pre-exponential amplitudes at different λ_τ and λ_t constitute 2D decay-associated spectra (2D DAS), which visually illustrate the dominant EET process occurring with a given lifetime (Figure 1B). Negative and positive peaks in the 2D DAS represent the decaying population (ground-state bleaching) of the donor states and the rising population of the acceptor states. However, care must be taken when oppositely signed induced absorption is also contributing to the dynamics.

Excitation dynamics at 77 K

The 2D electronic spectra of PSI (Figure 1) allow us to follow EET from the initially excited states, appearing along the diagonal line, predominantly to longer-wavelength Chls ($\lambda_t > \lambda_\tau$). Note that a cross-peak around 670→685 nm ($\lambda_\tau \rightarrow \lambda_t$) is already pronounced at 50 fs, which probably reflects both excitonic coupling as well as very fast relaxation – excitonic or vibrational – of states on the blue side of the absorption spectrum. Dynamic relaxation on a sub-100 fs timescale is evident in the kinetic traces in the cross-peak region (Supplementary Figure S4) and is consistent with RT fluorescence anisotropy measurements and theoretical modelling for PSI of *Thermosynechococcus elongatus*.[44-45, 56, 64-65]

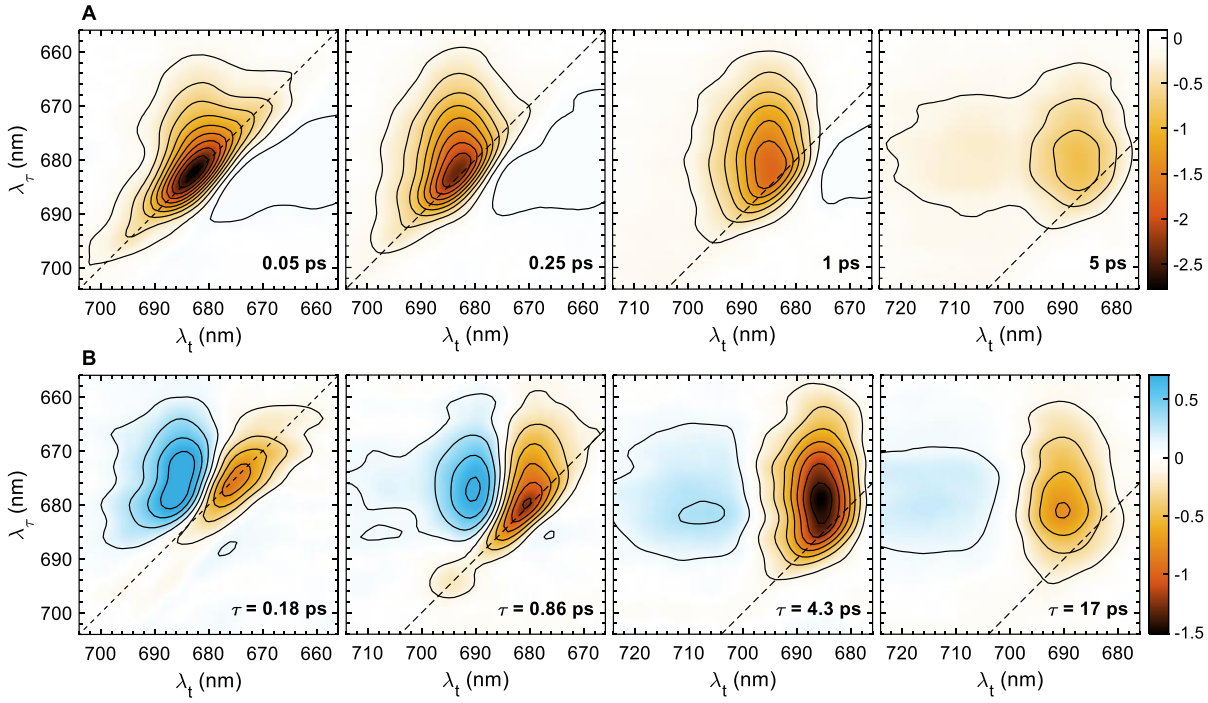

Figure 1. 2DES of minimal PSI at 77 K. A. Selected purely absorptive 2D electronic spectra at waiting times T_w indicated in the plots. The color scale corresponds to ΔA×10⁴ and the contour lines mark approximately 10% steps. B. 2D decay-associated spectra resulting from a five-exponential global fit. Negative/positive amplitudes represent decay/rise of the bleaching. The final 2D DAS corresponding to slow decay to the ground state is omitted.

In the time between 50 fs and 1 ps, short-wavelength diagonal signals decay and off-diagonal signals gain intensity as high-energy states relax to a subset of Chls absorbing around 685–690 nm. These EET components are better visualized by the 2D DAS resulted from global lifetime analysis of the 2DES data. The first component, with a 180 fs lifetime, shows mostly diagonal decay of directly excited states at wavelengths shorter than 680 nm and the second component, with a 0.86 ps lifetime, shows secondary EET (decaying cross-peak) to Chls absorbing around 690 nm. Subsequently, this pool of Chls decays with lifetimes of 4 ps and 17 ps, concomitant with the rise of red Chl signals at $\lambda_t \approx 710$ nm. The significantly larger decay amplitude at 690 nm compared to the rise at 710 nm, suggests that a fraction of the antenna excitations are trapped by the RC. The far-red signal continues to rise for as long as 40 ps and slowly decays thereafter (Supplementary Figure S4). This slow population of red Chls is consistent with time-resolved fluorescence measurements.[33] Finally, the decay of the long-wavelength bleaching occurs on a timescale longer than the experimental window (hundreds of ps to ns).

A lifetime close to 4 ps has been observed in virtually all earlier experiments on PSI from various organisms. It has been assigned to primary CS in the RC at RT[9, 17, 21, 25] and to EET to the red Chls at cryogenic temperatures.[32, 34-35] Including the present data, we can confirm that the same kinetic component is observed in PSI from green algae,[34-35] higher plants (unpublished data) and cyanobacteria.[32, 66] Not only the number but also the absorption maxima of the red Chls from these different PSI vary broadly. Therefore, it is unlikely that EET will occur with the same rates. On the other hand, the rise of the red Chls could simply follow the decay of the donor antenna states, depopulated by the RC. We therefore deem more likely that the dominant process in the 4 ps lifetime is photochemical.

For a more detailed look at the dynamics we take horizontal slices at different λ_τ and analyze them independently – by global lifetime analysis as well as lifetime density analysis, that transforms the data from population time domain into a range of exponential decay lifetimes.[17] The resulting one-dimensional decay-associated absorption difference spectra (DADS) and lifetime density maps for selected λ_τ are plotted in Figure 2 (additional plots in Supplementary Figure S5). The DADS can be compared to transient absorption studies on PSI from *Synechocystis*.[32, 66] Similar to the DADS, negative/positive amplitudes

in the lifetime density maps signify decay/rise of the bleaching (or rise/decay of induced absorption) occurring over a range of timescales. It can be seen in the 675 nm map that EET from higher-energy states spans from 30 fs to about 1 ps progressively populating longer-wavelength Chls. The shortest lifetimes (<100 fs) predominantly involve relaxation from around 670 nm to 680 nm. We stress that the sub-100 fs relaxation has a sizeable contribution – 45% of the total signal at 680 nm rises on this timescale upon 670 nm excitation (Supplementary Figure S5).

On a longer lifetime range (>1 ps), the lifetime density maps show virtually identical dynamics at all excitation wavelengths from 670 to 690 nm. The bleaching decays mostly on a timescale of 4–5 ps extending to 10–20 ps range. The position of the bleaching maximum of the 4–5 ps decay component is at $\lambda_t \approx 687$ nm irrespective of λ_τ. At the same time, the population of red Chls is seen as the positive-amplitude band at 700–720 nm.

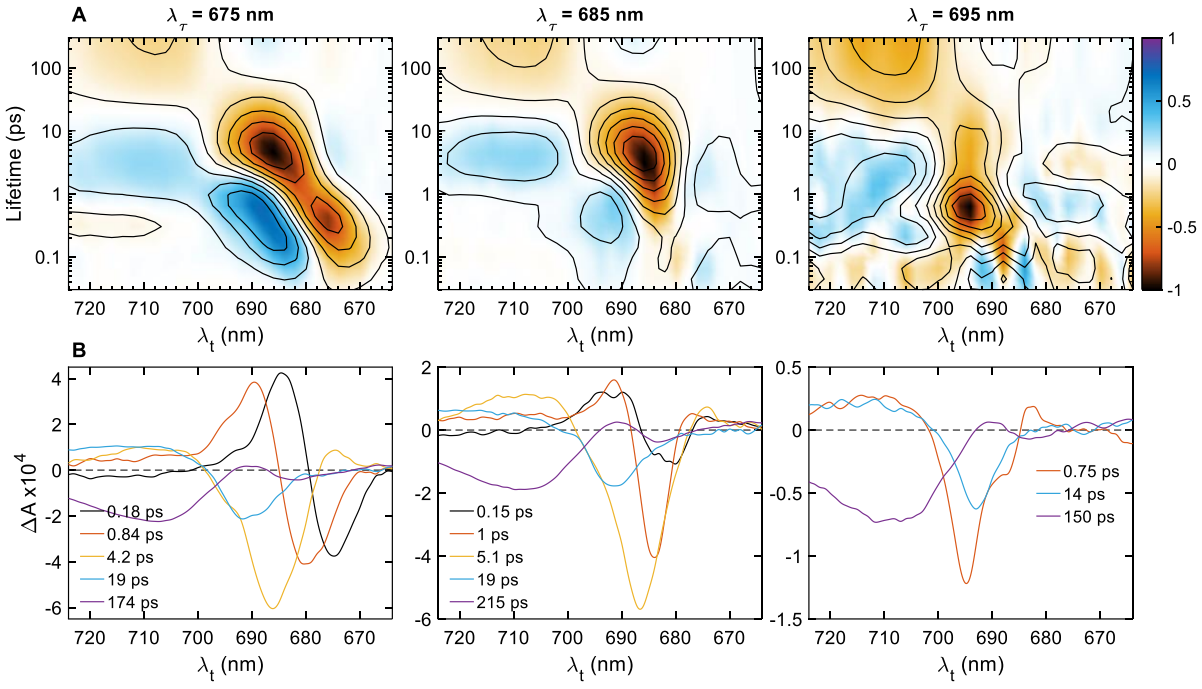

Figure 2. Lifetime analysis of slices of the 2DES data at selected excitation wavelength λ_τ. A. Lifetime density maps, representing the dynamics at different detection wavelengths λ_t starting with a selected λ_τ in a lifetime domain (in logarithmic scale). Negative/positive amplitudes represent decay/rise of bleaching (color scale in normalized ΔA units). B. Decay-associated absorption difference spectra, resulting from a 3–5-exponential fit of the traces at given λ_τ. The final lifetimes exceeding the measurement range (100 ps) are not accurately determined.

To facilitate interpretation, we also compare evolution-associated difference spectra (EADS) obtained by fitting a sequential kinetic model to the 2D slices (Supplementary Figure S6). The spectra show the progressive formation of lower-energy states with lifetimes from 70 fs to 1.4 ps, depending on the initial excitation. Irrespective of excitation wavelength, a spectrum decaying on a 4–5 ps timescale shows a broader shape with a maximum at 687 nm.

Fast decay of red-edge excitations

Compared to the excitation of the bulk antenna, direct excitation at 695 nm – at the red edge of the absorption spectrum – triggers radically different dynamics. In this case a narrowband transient hole (150 cm^{-1} FWHM) is formed (Figure 2B) that decays with a lifetime of 0.7–0.8 ps. The fast decay of the diagonal signal at 695 nm is evident in the kinetic traces (Supplementary Figure S4), 2D DAS (Figure 1), lifetime density maps and DADS (Figure 2). The decay of the initial narrow bleaching spectrum leads to the formation of a broader spectrum with a maximum at 702 nm (see Supplementary Figure S6, λ_τ = 695 nm). Excitation at 700 nm produces a bimodal spectrum with a broad asymmetric band at 700 nm accompanied by a resonant

photobleaching band at 683 nm, that also decays on a sub-ps timescale (Supplementary Figure S6, λ_τ = 700 nm). The spectrum, reminiscent of the $P_{700}^+ - P_{700}$ absorption difference spectrum,[66] can be ascribed to the RC.[34]

The qualitative change in the excited-state dynamics can be explained if we assume that excitation at 695–700 nm preferentially targets the RC Chls which engage in a photochemical reaction. At low temperature, at least half of the PSI complexes have permanently oxidized P_{700}, whereas in the other half, recombination of $P_{700}^+A_1^-$ occurs within the 2-ms period between pulses.[31] It is then reasonable to propose that excitation of the RC Chls is followed by rapid CS and a formation of primary radical pairs that could include $P_{700}^+A_0^-$ and $A^+A_0^-$. Several studies have suggested that Chls in the RC absorb at 692–695 nm.[32, 67-68] The spectrally narrow transient hole at 695 nm can be assigned to an exciton state most probably localized on Chls eC_2 or eC_3, while the subsequent broad bleaching at 700–705 nm most likely reflects P_{700}^+. Therefore, at 77 K the 0.7–0.8 ps lifetime represents the effective CS rate of the RC (1.2–1.5 ps^{-1}). We cannot determine with certainty whether this process involves two subsequent steps of exciton relaxation from the 695 nm state followed by very fast CS, or direct charge transfer from a donor different than P_{700}.

In summary, the data indicate that EET to the RC is substantially slower than the primary CS at 77 K. Upon antenna excitation, both the trapping time and the spectrum of the decaying component – with a maximum at 687 nm – are independent of excitation wavelength. This strongly indicates a kinetic "bottleneck" at a small pool of antenna Chls. It is tempting to assign the bottleneck as "transfer-to-trap", owing to the relatively long distance between the antenna Chls and the RC. However, structure-based modelling indicates that the limiting factor is the excitation energy and not the distance to the RC (see below).

Dynamics at room temperature

As an added control, we recorded 2D electronic spectra from the minimal PSI at RT. Representative 2D spectra are shown in Supplementary Figure S7. Global analysis resolved four exponential decay and one non-decaying component. The lifetimes and 2D DAS (Figure 3) are very similar to those obtained from trimeric *Synechocystis* PCC 6803 reported by Lee, et al. [45] The first two lifetimes, 80 fs and 0.5 ps show exciton equilibration in the antenna with uphill and downhill EET components. This is followed by two trapping lifetimes of 3.6 and 22 ps. The former presents a cross-peak reflecting rising population of red Chls.

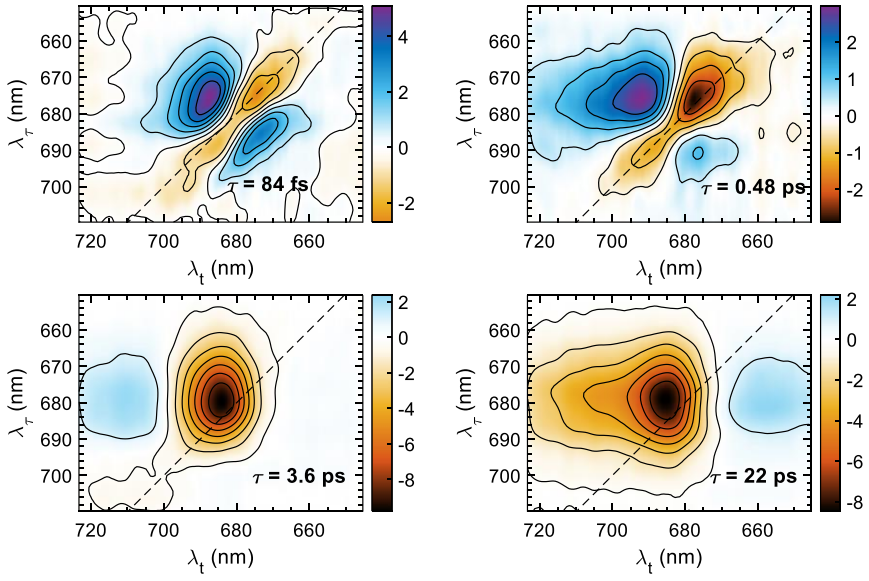

Figure 3. 2D decay-associated spectra (2D DAS) of PSI from *Synechocystis* ΔFIJL resulting from a five-exponential fit of the 2D electronic spectra recorded at RT. The positive/negative amplitudes are represented in blue/red colors and correspond to ΔA×10^4). The 2D DAS corresponding to a non-decaying component is omitted.

The early-time dynamics is very similar in plant PSI, including the 3-ps 2D DAS, but overall trapping is slowed down by equilibration with the peripheral antenna.[26] Excluding red Chls from the PSI core, we could explain these results with a model wherein the 3 ps lifetime is dominated by the rate of primary CS equal to ~0.4 ps^{-1}, similar to previous models by Holzwarth and coworkers.[21, 25] Virtually the same model could fit the RT kinetics of cyanobacterial PSI if we include EET to red Chls (not shown). To reconcile the results at different temperatures it must be then assumed that the primary CS rate in the RC is approx. three times slower at RT than at 77 K while the transfer to the RC is correspondingly faster. An acceleration of energy transfer at RT is to be expected according to theoretical calculations as well as experimental results.[36-38] It is also within expectations that the effective CS rate at RT is slower – assuming that energy can rapidly equilibrate among all RC Chls making them effectively degenerate. The intrinsic CS rate should then be divided by an entropy factor equal to the number of degenerate states. In this case, the kinetics becomes trap-limited with a higher probability that RC excitations escape to the antenna. In either case, simple kinetic calculations can show that even if the CS rate at RT is still 1.2 ps^{-1}, the kinetics would not be diffusion-limited but there would be almost even chances for excitations on the RC to be trapped by CS or de-trapped by the antenna.

The excitation dynamics at 77 K and RT are summarized in a schematic (Supplementary Figure 11). Excitations on higher-energy Chls (670–680 nm) are concentrated on a subpicosecond timescale to subset of red-shifted Chls. The states absorbing at 687 nm are depopulated within 4 ps by both the RC and transfer to red Chls. The lifetime is equal to the inverse of the sum of all relaxation rate constants, but the dominant pathway is likely to the RC. Once energy reaches the RC Chls (red-outlined ovals), CS occurs with a time constant of ~0.8 ps followed by secondary electron transfer to A_1. The latter likely contributes to the loss of bleaching at ~680 nm (Chl A_0) on a 10–20 ps timescale.

Structure-based model of EET

For a better understanding of the dynamics and to support the interpretation of the 2DES results, we performed structure-based modelling of EET. To this end, the structure of the minimal PSI complex was determined by cryo-EM and refined and built based on the high-resolution structure of trimeric PSI from *Synechocystis* PCC 6803.[6] This allowed us to resolve not only the seven protein subunits (Figure 4) but also the 88 coordinated Chl *a* molecules, as well as 17 carotenoids, two phylloquinones (A_1), three Fe-S clusters (F_A, F_B, F_X) and nine lipids. Overall, the minimal PSI retained a very similar structure with the corresponding parts of the trimeric PSI (Supplementary Figure S8), which explains the similar spectroscopic and dynamic behaviour.[33] Nevertheless, differences in the geometry of the Chls can be observed, especially in the monomerization region, that have an effect on the excitonic couplings (see below).

Several structure-based dynamic models of PSI have been proposed, with the rates of EET calculated using Förster or generalized Förster theory,[56, 69-70] Redfield theory, or hierarchical equations of motion.[71] Previously, we have shown that Förster theory alone can qualitatively describe the equilibration with red Chls at 77 K in the tens to hundreds of picoseconds range,[33] however, we omitted any details on the faster processes. Here we present computations on the recently resolved structure of the minimal PSI complex using a combined Redfield-Förster approach, as developed and applied to other photosynthetic complexes in the past.[55]

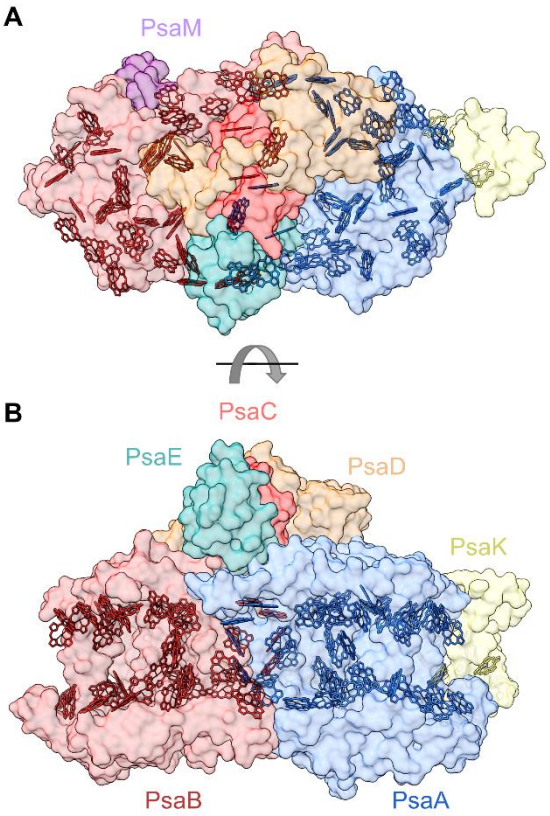

Figure 4. Structure of the ΔFIJL PSI complex (PDB ID 701V). The colored surfaces represent the apoprotein subunits and the chlorin rings of the 88 chlorophyll *a* molecules are shown as sticks. A. Top view. B. Membrane view.

The largest excitonic couplings of the minimal PSI are compared in Supplementary Table S3 with the values in trimeric PSI from wild type *Synechocystis* PCC 6803 and *Thermosynechococcus elongatus*. The largest relative change in excitonic coupling in the minimal complex is between Chls A32 and B7 – the coupling is 50 and 80% stronger in the trimeric PSI from *Synechocystis* PCC 6803 and *T. elongatus,* respectively. Based on analysis of the fluorescence spectra of PSI, we predicted that the environment alters the excitonic coupling between Chls A32-B7 and, consequently, this pair no longer contributes to the long-wavelength emission in monomeric PSI types.[33] Thus, the present finding strongly supports our earlier assignment.

The modelled steady-state spectra compared very well with the experimental data (Supplementary Figure S9). The calculation predicted rapid exciton relaxation in the RC as well as among strongly coupled Chls on the PsaA and PsaB branch and the connectivity scheme is in good agreement with earlier calculations on PSI from *T. elongatus*.[71] Figure 5 illustrates the EET connectivity and the site population calculated for two waiting times, 50 fs and 5 ps, after excitation at either 675 nm or 697 nm. The time-dependent population of Chl groups is plotted in Supplementary Figure S10 and exponential decay lifetimes are shown in Supplementary Table S4. The initially excited pool after 675 nm excitation consists of mostly high-energy Chls but after 5 ps, the excitations have transferred to a smaller pool of red-shifted Chls, with almost half of the excitations found on 10–12 Chls having peak wavelengths in the range 685–690 nm. In contrast, excitation at 697 populates predominantly the RC Chls and, to a lesser extent, the red Chls pairs B31–B32 and B37–B38 (see also Supplementary Figure S9). The RC population decays within a few ps because of the presumed CS rate of 1.5 ps^{-1}.

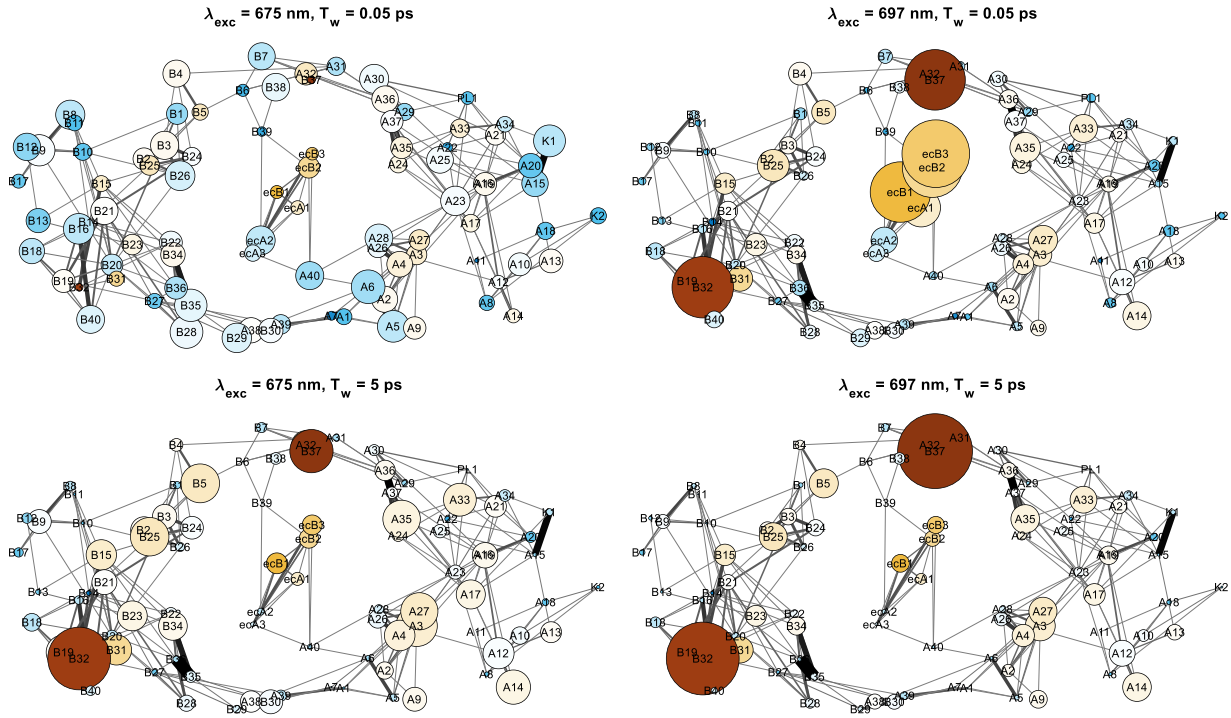

Figure 5. Structure-based Redfield-Förster model of EET in PSI. Circles represent the population of individual Chls calculated for waiting times 50 fs and 5 ps after excitation at 675 nm or 697 nm, with the Chl site energies indicated by the circle colors. Lines represent EET between Chls with the line weight indicating the rate. Excitation at 675 nm intersects mainly high-energy Chls (blue), whereas 695 nm light predominantly excites the RC and red Chls. After 5 ps, excitations are concentrated on a smaller pool of low-energy Chls (yellow-red).

The model dynamics compares remarkably well with the experimental data, as demonstrated by the simulated lifetime density maps and DADS (Figure 6). Note that the simulation includes neither coherent dynamics nor photoinduced absorption (including absorption of radical pairs). In agreement with the 2DES results, excitation on the blue side of the absorption band is followed by gradual downhill EET among Chls absorbing in the 670–680 nm range on timescales spanning ca. 0.1–1 ps. Irrespective of the excitation wavelength, the main excitation decay occurs from states around 688 nm on timescales 5–20 ps, concomitant with the rise of red Chls. In this time range, the model dynamics lags compared to the experimental, indicating that the Förster EET rates are underestimated. Nonetheless, we now understand the reason for the kinetic limitation being the slow EET from low-energy Chls absorbing in the range 685–690 nm and acting as pseudotraps.

A crucial characteristic of the model is that wavelengths longer than 695 nm excite predominantly the RC in the minimal PSI, resulting in a rapid excitation decay with a dominant lifetime equal to the inverse primary CS rate. The lowest exciton states belonging to the six RC Chls absorb around 696 and 700 nm. Upon excitation in this wavelength region, the dynamics reflects both exciton equilibration and decay. The experimental DADS of the 0.7 ps component differ from the model in that it has pronounced positive amplitude at λ_t > 700 nm. This most likely indicates the formation of the charge-separated state (P_{700}^+), which is not explicitly modelled.

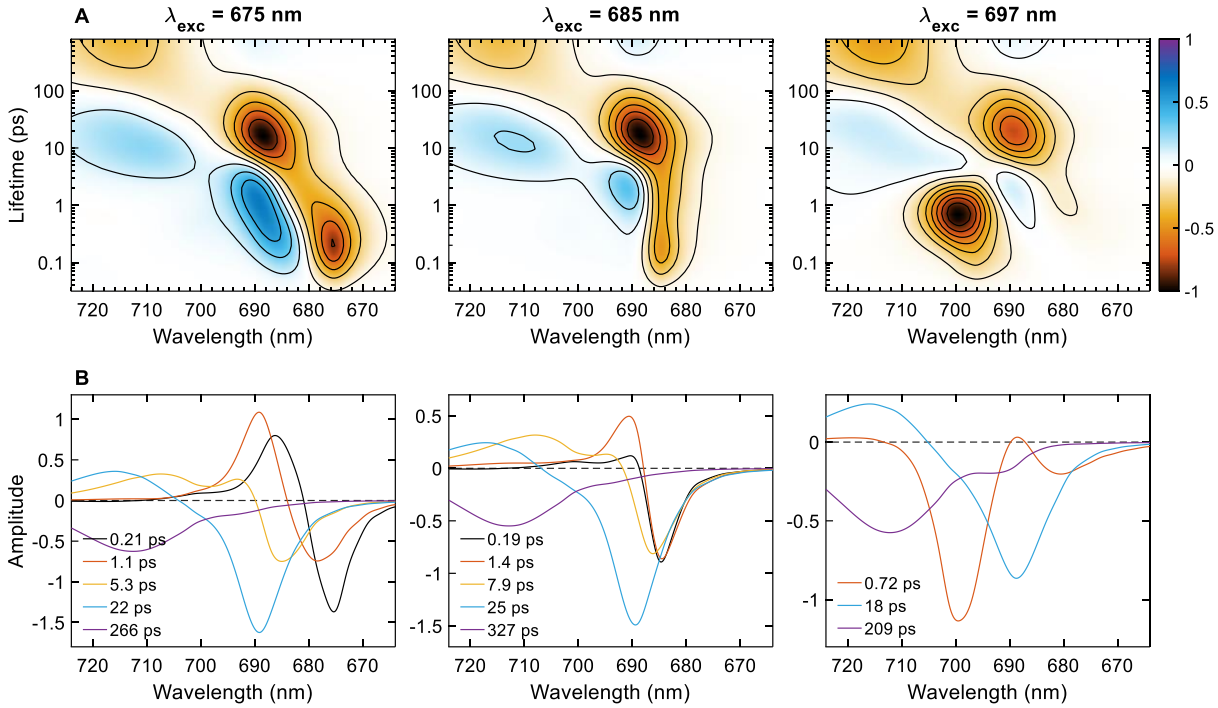

Figure 6. Simulated excitation dynamics of PSI at 77 K after excitation at 675, 685 or 697 nm. A. Lifetime density maps of the wavelength-resolved absorptive signal. B. Decay-associated absorption difference spectra.

In summary, the 2DES results and the structure-based modelling show that the kinetics of PSI at 77 K is largely limited by EET from a small pool of red-shifted Chls to the RC, which is about one order of magnitude slower than the primary CS. A simplified kinetic scheme is shown in Figure 7, indicating the main timescales of EET between Chl pools at 77 K and RT. CS is the sum of the intrinsic one-step CS rates to different primary acceptors.[21] From the 2DES we obtained a primary CS rate of 1.2 ps^{-1}, which is in line with several predictions from theoretical[19, 72] and experimental studies at RT.[11, 20] A comparably fast CS at cryogenic temperature would mean that electron transfer is activationless, i.e. the free energy of the reaction is of the same magnitude as the reorganization energy. Such is the case for the purple bacterial RC, where primary CS accelerates at low temperatures (see ref.[12] and refs. therein). Note, however, that even if the intrinsic CS rate is the same at RT, the effective CS time upon RC excitation should be longer because of equilibration among several (3–6) Chls.[21]

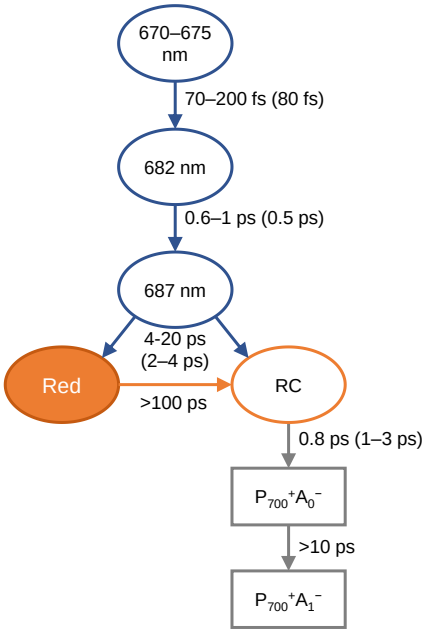

Figure 7. Schematic diagram of the energy and electron transfer dynamics in PSI. The ovals represent bulk antenna Chl pools absorbing around the indicated wavelengths, the red Chls and the RC Chls. The rectangles represent charge-separated states. The numbers next to the arrows indicate the effective transfer timescales at 77 K obtained from analysis of the 2DES data (the numbers in parentheses correspond to room temperature).

Quantum coherence

One of the central themes of research in the primary processes of photosynthesis in the past decade has been to establish the role of quantum coherence in photosynthesis.[41-43, 73] According to the current scientific consensus, purely electronic coherences between excitons are not likely to be long-living [42] and hence not involved in energy transfer processes. Studies indicate that exciton–vibrational (vibronic) coherence is involved in the efficiency of CS in both the purple bacterial RC and Photosystem II.[43] This is based on long-lived coherences observed by 2DES [74-76] and predicted by theory as the outcome of coupling of excitonic and charge-transfer states in the RC via resonant vibrational modes. However, proving and assigning vibrational modes to the associated processes is exceedingly difficult and requires detailed analysis performed globally on the relative phases and amplitudes of multiple diagonal and cross-peaks.[77-78] Despite the difficulties, as a first step, it is useful to identify potential vibrational modes that may be coupled to the excitonic states.

It is much harder to selectively observe coherent oscillations in the native PSI in the background of a large number of antenna Chls. Nonetheless, we recorded 2D electronic spectra of the subunit-depleted PSI with 10 fs time step. Visual inspection hardly reveals any oscillations in the noisy kinetics, but the Fourier-transformed data (See Supplementary Figure S11) reveals 2D FT maps (Figure 8) with distinct features at ω_t = 243 cm^{-1} and 104 cm^{-1} (The axes have been changed to wavenumbers to allow a more intuitive visualization of the locations of the cross-peaks).

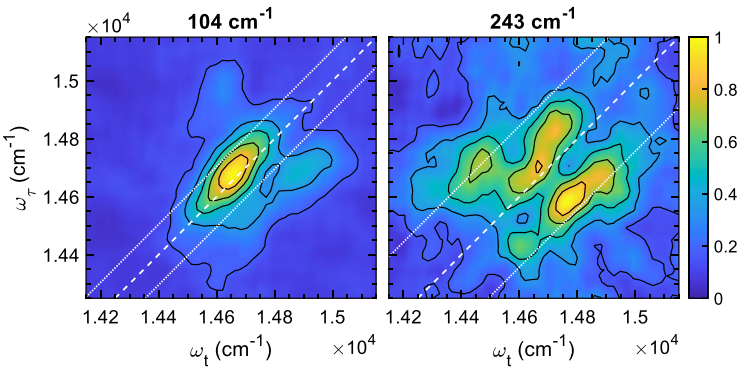

Figure 8. FT 2D frequency correlation maps for two selected oscillation frequencies, 104 and 243 cm^{-1}. The maps indicate regions in the 2D electronic spectrum that oscillate along T_w with the given frequency. The 2DES are Fourier-transformed along waiting time T_w and the absolute-valued transformed data are sliced at the selected frequencies to obtain the maps. Note that the excitation and detection axes are in cm^{-1}. The dotted white lines indicate an offset of ±104 and ±243 cm^{-1}, respectively, from the diagonal.

In the 243 cm^{-1} frequency map, one can distinctly see multiple peaks situated at $(\omega_\tau, \omega_t) = (\omega_{eg} \pm 0, \omega_0, \omega_{eg} \pm 0, \omega_0)$, where ω_{eg} = 14,680 cm^{-1} (681 nm) corresponds to the lower frequency range of the antennae Chls absorption and ν_0 denotes the oscillation frequency. The peak positions are consistent with the oscillational patterns arising from vibronic origins [79]. Within the error of the 243 cm^{-1} map (~33 cm^{-1} resolution), this may well correspond to a 262 cm^{-1} vibrational mode frequency present in Chl *a* molecules [80]. We can therefore assign the 243 cm^{-1} map to a vibronic origin of the Chl *a* chromophores. In the 104 cm^{-1} frequency map, a peak along the diagonal can be clearly seen (Figure 8) centred also at ν_{eg} = 14,680 cm^{-1} (681 nm). As the beating frequency at 104 cm^{-1} is low, the absolute valued frequency map cannot resolve the individual peaks as well as the 243-cm^{-1} frequency map does. Beating patterns at these frequencies are also observed in 2DES studies in the Chl *a* monomers [81].

Conclusions

In this work we performed 2DES of a minimal PSI complex using very low pulse energies to avoid singlet annihilation, while recording the kinetics with high dynamic range. These data, together with the structure-based calculations using Redfield-Förster theory, provide extraordinary rich and detailed information about the dynamics of energy and electron transfer. Structure-based calculations indicated impaired excitonic couplings between Chls in the monomerization region, especially A32–B7, which might be the main reason for the reduced far-red absorption of the monomeric PSI. The high quantum yield of photochemical energy conversion in PSI is in part due to the fast EET among its tightly packed antenna Chls, with hopping times under 100 fs. At 77 K antenna excitations are funnelled within 1 ps to a small pool of Chls having peak absorption at 685–690 nm. These lower-energy states constitute a kinetic bottleneck of the overall excitation trapping by the RC which occurs on timescales of 4–20 ps. The very fast CS at 77 K indicates an unusual temperature dependence of electron transfer that is reminiscent of the purple bacterial RC. The rate of primary CS observed upon direct excitation of the RC is 1.2–1.5 ps^{-1} and involves a previously unresolved exciton state absorbing around 695 nm. More work is needed to clarify the physical nature and mechanism of relaxation of this state. Analysis of quantum beats in the 2D electronic spectra suggest that they are of vibronic origins at ~100 cm^{-1} and ~250 cm^{-1}, possibly associated with vibrations in Chls absorbing near 681 nm. It remains an open question whether the observed oscillations represent coherences within the electron-transport chain as in other types of RCs. [74-75]

ASSOCIATED CONTENT

Supporting Information. Supporting figures, theory for calculating optical spectra. This material is available free of charge via the Internet at http://pubs.acs.org.

Data availability. The atomic coordinates of the model have been deposited in the Protein Data Bank, with accession codes 7O1V. The cryo-EM map has been deposited in the Electron Microscopy Data Bank, with accession codes EMD-12697.

Author information

Corresponding authors

Petar H. Lambrev, Biological Research Centre, Szeged, Temesvári krt. 62, Szeged 6726, Hungary, lambrev.petar@brc.hu; Howe-Siang Tan, School of Physical and Mathematical Sciences, Nanyang Technological University, Nanyang Link 21, Singapore, HoweSiang@ntu.edu.sg

‖ Present address: The Robert H. Smith Institute of Plant Sciences and Genetics in Agriculture, The Hebrew University of Jerusalem, Rehovot, Israel

Funding sources

This work was supported by grants from the National Research, Development and Innovations Office, Hungary (NKFIH 2018-1.2.1-NKP-2018-000009 to P.L.), Eötvös Loránd Research Network (KÖ-37/2020 to P.L.) and the Singapore Ministry of Education Academic Research Fund (Tier 1 RG2/19 and Tier 1 RG14/20 to H.-S.T.). N.N. acknowledges support by The Israel Science Foundation (Grant No. 569/17), and by German-Israeli Foundation for Scientific Research and Development (GIF), Grant no. G-1483-207/2018.

Acknowledgements

The authors are grateful to Prof. Dr. Thomas Renger for the valuable discussions. The authors acknowledge Diamond Light Source for access and support of the cryo-EM facilities at the UK's National Electron Bio-imaging Centre (under proposal EM BI21643-1), funded by the Wellcome Trust, MRC and BBSRC. Molecular graphics and analyses were performed with ChimeraX, developed by the Resource for Biocomputing, Visualization, and Informatics at the University of California, San Francisco, with support from National Institutes of Health R01-GM129325 and the Office of Cyber Infrastructure and Computational Biology, National Institute of Allergy and Infectious Diseases.

References

1. Fromme, P.; Jordan, P.; Krauß, N., Structure of photosystem I. *Biochim. Biophys. Acta* **2001,** *1507* (1–3), 5–31.
2. Golbeck, J. H., The binding of cofactors to photosystem I analyzed by spectroscopic and mutagenic methods. *Annu. Rev. Biophys. Biomol. Struct.* **2003,** *32* (1), 237–256.
3. Nelson, N.; Junge, W., Structure and energy transfer in photosystems of oxygenic photosynthesis. *Annu. Rev. Biochem.* **2015,** *84*, 659–683.
4. Jordan, P.; Fromme, P.; Witt, H. T.; Klukas, O.; Saenger, W.; Krauß, N., Three-dimensional structure of cyanobacterial photosystem I at 2.5 Å resolution. *Nature* **2001,** *411* (6840), 909–917.
5. Mazor, Y.; Nataf, D.; Toporik, H.; Nelson, N., Crystal structures of virus-like photosystem I complexes from the mesophilic cyanobacterium *Synechocystis* PCC 6803. *Elife* **2014,** *3*, e01496.
6. Malavath, T.; Caspy, I.; Netzer-El, S. Y.; Klaiman, D.; Nelson, N., Structure and function of wild-type and subunit-depleted photosystem I in *Synechocystis*. *Biochim. Biophys. Acta* **2018,** *1859* (9), 645–654.
7. Karapetyan, N. V.; Schlodder, E.; van Grondelle, R.; Dekker, J. P., The long-wavelength chlorophylls of photosystem I. In *Photosystem I: The Light-Driven, Plastocyanin:Ferredoxin Oxidoreductase*, Golbeck, J. H., Ed. Springer: Dordrecht, The Netherlands, 2006; pp 177–192.
8. Gobets, B.; van Grondelle, R., Energy transfer and trapping in photosystem I. *Biochim. Biophys. Acta* **2001,** *1507* (1–3), 80–99.
9. Hastings, G.; Kleinherenbrink, F. A.; Lin, S.; Blankenship, R. E., Time-resolved fluorescence and absorption spectroscopy of photosystem I. *Biochemistry* **1994,** *33* (11), 3185–3192.
10. Melkozernov, A. N.; Lin, S.; Blankenship, R. E., Excitation dynamics and heterogeneity of energy equilibration in the core antenna of photosystem I from the cyanobacterium *Synechocystis sp.* PCC 6803. *Biochemistry* **2000,** *39* (6), 1489–1498.
11. Savikhin, S.; Xu, W.; Chitnis, P. R.; Struve, W. S., Ultrafast primary processes in PS I from *Synechocystis sp*. PCC 6803: roles of P_{700} and A_0. *Biophys. J.* **2000,** *79* (3), 1573–1586.
12. Savikhin, S.; Jankowiak, R., Mechanism of Primary Charge Separation in Photosynthetic Reaction Centers. In *The Biophysics of Photosynthesis*, Golbeck, J.; van der Est, A., Eds. Springer New York: 2014; Vol. 11, pp 193–240.
13. Melkozernov, A. N., Excitation energy transfer in Photosystem I from oxygenic organisms. *Photosynth. Res.* **2001,** *70* (2), 129–153.

14. Croce, R.; van Amerongen, H., Light-harvesting in photosystem I. *Photosynth. Res.* **2013,** *116* (2–3), 1–14.
15. Holzwarth, A. R.; Schatz, G.; Brock, H.; Bittersmann, E., Energy transfer and charge separation kinetics in photosystem I: Part 1: Picosecond transient absorption and fluorescence study of cyanobacterial photosystem I particles. *Biophys. J.* **1993,** *64* (6), 1813.
16. Melkozernov, A. N.; Su, H.; Webber, A. N.; Blankenship, R. E., Excitation energy transfer in thylakoid membranes from *Chlamydomonas reinhardtii* lacking chlorophyll *b* and with mutant photosystem I. *Photosynth. Res.* **1998,** *56* (2), 197–207.
17. Müller, M. G.; Niklas, J.; Lubitz, W.; Holzwarth, A. R., Ultrafast transient absorption studies on photosystem I reaction centers from *Chlamydomonas reinhardtii*. 1. A new interpretation of the energy trapping and early electron transfer steps in photosystem I. *Biophys. J.* **2003,** *85* (6), 3899–3922.
18. Valkunas, L.; Liuolia, V.; Dekker, J. P.; Grondelle, R., Description of energy migration and trapping in photosystem I by a model with two distance scaling parameters. *Photosynth. Res.* **1995,** *43* (2), 149–154.
19. Beddard, G., Excitations and excitons in photosystem I. *Phil. Trans. R. Soc. London Ser. A* **1998,** *356* (1736), 421–448.
20. Kumazaki, S.; Ikegami, I.; Furusawa, H.; Yasuda, S.; Yoshihara, K., Observation of the excited state of the primary electron donor chlorophyll (P700) and the ultrafast charge separation in the spinach Photosystem I reaction center. *J. Phys. Chem. B* **2001,** *105* (5), 1093–1099.
21. Müller, M. G.; Slavov, C.; Luthra, R.; Redding, K. E.; Holzwarth, A. R., Independent initiation of primary electron transfer in the two branches of the photosystem I reaction center. *Proc. Natl. Acad. Sci. U.S.A.* **2010,** *107* (9), 4123–4128.
22. Andrizhiyevskaya, E. G.; Frolov, D.; van Grondelle, R.; Dekker, J. P., Energy transfer and trapping in the photosystem I complex of *Synechococcus* PCC 7942 and in its supercomplex with IsiA. *Biochim. Biophys. Acta* **2004,** *1656* (2–3), 104–113.
23. Gibasiewicz, K.; Ramesh, V. M.; Melkozernov, A. N.; Lin, S.; Woodbury, N. W.; Blankenship, R. E.; Webber, A. N., Excitation dynamics in the core antenna of PS I from *Chlamydomonas reinhardtii* CC 2696 at room temperature. *J. Phys. Chem. B* **2001,** *105*, 11498–11506.
24. Holzwarth, A. R.; Müller, M. G.; Niklas, J.; Lubitz, W., Charge recombination fluorescence in photosystem I reaction centers from *Chlamydomonas reinhardtii*. *J. Phys. Chem. B* **2005,** *109* (12), 5903–5911.
25. Slavov, C.; Ballottari, M.; Morosinotto, T.; Bassi, R.; Holzwarth, A. R., Trap-limited charge separation kinetics in higher plant photosystem I complexes. *Biophys. J.* **2008,** *94*, 3601–3612.
26. Akhtar, P.; Zhang, C.; Liu, Z.; Tan, H.-S.; Lambrev, P. H., Excitation transfer and trapping kinetics in plant photosystem I probed by two-dimensional electronic spectroscopy. *Photosynth. Res.* **2018,** *135* (1–3), 239–250.
27. Russo, M.; Petropoulos, V.; Molotokaite, E.; Cerullo, G.; Casazza, A. P.; Maiuri, M.; Santabarbara, S., Ultrafast excited-state dynamics in land plants Photosystem I core and whole supercomplex under oxidised electron donor conditions. *Photosynth. Res.* **2020,** *144* (2), 221–233.
28. Shelaev, I. V.; Gostev, F. E.; Mamedov, M. D.; Sarkisov, O. M.; Nadtochenko, V. A.; Shuvalov, V. A.; Semenov, A. Y., Femtosecond primary charge separation in *Synechocystis* sp. PCC 6803 photosystem I. *Biochim. Biophys. Acta* **2010,** *1797* (8), 1410–1420.
29. Cherepanov, D. A.; Shelaev, I. V.; Gostev, F. E.; Mamedov, M. D.; Petrova, A. A.; Aybush, A. V.; Shuvalov, V. A.; Semenov, A. Y.; Nadtochenko, V. A., Mechanism of adiabatic primary electron transfer in photosystem I: Femtosecond spectroscopy upon excitation of reaction center in the far-red edge of the Q_Y band. *Biochim. Biophys. Acta* **2017,** *1858* (11), 895–905.
30. Pålsson, L.-O.; Flemming, C.; Gobets, B.; van Grondelle, R.; Dekker, J. P.; Schlodder, E., Energy transfer and charge separation in photosystem I: P_{700} oxidation upon selective excitation of the long-wavelength antenna chlorophylls of *Synechococcus elongatus*. *Biophys. J.* **1998,** *74* (5), 2611–2622.
31. Schlodder, E.; Falkenberg, K.; Gergeleit, M.; Brettel, K., Temperature dependence of forward and reverse electron transfer from A_1^-, the reduced secondary electron acceptor in photosystem I. *Biochemistry* **1998,** *37* (26), 9466–9476.
32. Melkozernov, A. N.; Lin, S.; Blankenship, R. E.; Valkunas, L., Spectral inhomogeneity of photosystem I and its influence on excitation equilibration and trapping in the cyanobacterium *Synechocystis* sp. PCC6803 at 77 K. *Biophys. J.* **2001,** *81* (2), 1144–1154.
33. Akhtar, P.; Biswas, A.; Kovacs, L.; Nelson, N.; Lambrev, P. H., Excitation energy transfer kinetics of trimeric, monomeric and subunit-depleted Photosystem I from *Synechocystis* PCC 6803. *Biochem. J.* **2021,** *478* (7), 1333–1346.
34. Gibasiewicz, K.; Ramesh, V. M.; Lin, S.; Woodbury, N. W.; Webber, A. N., Excitation dynamics in eukaryotic PS I from *Chlamydomonas reinhardtii* CC 2696 at 10 K. Direct detection of the reaction center exciton states. *J. Phys. Chem. B* **2002,** *106* (24), 6322–6330.
35. Melkozernov, A. N.; Kargul, J.; Lin, S.; Barber, J.; Blankenship, R. E., Spectral and kinetic analysis of the energy coupling in the PS I–LHC I supercomplex from the green alga *Chlamydomonas reinhardtii* at 77 K. *Photosynth. Res.* **2005,** *86* (1–2), 203–216.
36. Jia, Y.; Jean, J. M.; Werst, M. M.; Chan, C.-K.; Fleming, G. R., Simulations of the temperature dependence of energy transfer in the PSI core antenna. *Biophys. J.* **1992,** *63* (1), 259–273.
37. van Grondelle, R.; Dekker, J. P.; Gillbro, T.; Sundstrom, V., Energy transfer and trapping in photosynthesis. *Biochim. Biophys. Acta* **1994,** *1187* (1), 1–65.
38. Leng, X.; Do, T. N.; Akhtar, P.; Nguyen, H. L.; Lambrev, P.; Tan, H. S., Hierarchical equations of motion simulation of temperature-dependent two-dimensional electronic spectroscopy of the chlorophyll *a* manifold in LHCII. *Chemistry—An Asian Journal* **2020,** *15* (13), 1996–2004.
39. Schlau-Cohen, G. S.; Ishizaki, A.; Fleming, G. R., Two-dimensional electronic spectroscopy and photosynthesis: Fundamentals and applications to photosynthetic light-harvesting. *Chem. Phys.* **2011,** *386* (1–3), 1–22.
40. Lambrev, P. H.; Akhtar, P.; Tan, H.-S., Insights into the mechanisms and dynamics of energy transfer in plant light-harvesting complexes from two-dimensional electronic spectroscopy. *Biochim. Biophys. Acta* **2020,** *1861* (4), 148050.
41. Ishizaki, A.; Fleming, G. R., Quantum coherence in photosynthetic light harvesting. *Annu. Rev. Condens. Matter Phys.* **2012,** *3* (1), 333–361.
42. Cao, J.; Cogdell, R. J.; Coker, D. F.; Duan, H.-G.; Hauer, J.; Kleinekathöfer, U.; Jansen, T. L. C.; Mančal, T.; Miller, R. J. D.; Ogilvie, J. P.; Prokhorenko, V. I.; Renger, T.; Tan, H.-S.; Tempelaar, R.; Thorwart, M.; Thyrhaug, E.; Westenhoff, S.; Zigmantas, D., Quantum biology revisited. *Sci. Adv.* **2020,** *6* (14), eaaz4888.
43. Romero, E.; Novoderezhkin, V. I.; van Grondelle, R., Quantum design of photosynthesis for bio-inspired solar-energy conversion. *Nature* **2017,** *543* (7645), 355.

44. Anna, J. M.; Ostroumov, E. E.; Maghlaoui, K.; Barber, J.; Scholes, G. D., Two-dimensional electronic spectroscopy reveals ultrafast downhill energy transfer in photosystem I trimers of the cyanobacterium *Thermosynechococcus elongatus*. *J. Phys. Chem. Lett.* **2012,** *3* (24), 3677–3684.
45. Lee, Y.; Gorka, M.; Golbeck, J. H.; Anna, J. M., Ultrafast Energy Transfer Involving the Red Chlorophylls of Cyanobacterial Photosystem I Probed through Two-Dimensional Electronic Spectroscopy. *J. Am. Chem. Soc.* **2018,** *140* (37), 11631–11638.
46. Nowakowski, P. J.; Khyasudeen, M. F.; Tan, H.-S., The effect of laser pulse bandwidth on the measurement of the frequency fluctuation correlation functions in 2D electronic spectroscopy. *Chem. Phys.* **2018,** *515*, 214–220.
47. Zhang, Z.; Wells, K. L.; Hyland, E. W. J.; Tan, H.-S., Phase-cycling schemes for pump–probe beam geometry two-dimensional electronic spectroscopy. *Chem. Phys. Lett.* **2012,** *550*, 156–161.
48. Zheng, S. Q.; Palovcak, E.; Armache, J.-P.; Verba, K. A.; Cheng, Y.; Agard, D. A., MotionCor2: anisotropic correction of beam-induced motion for improved cryo-electron microscopy. *Nat. Methods* **2017,** *14* (4), 331-332.
49. Zivanov, J.; Nakane, T.; Forsberg, B. O.; Kimanius, D.; Hagen, W. J.; Lindahl, E.; Scheres, S. H., New tools for automated high-resolution cryo-EM structure determination in RELION-3. *elife* **2018,** *7*, e42166.
50. Emsley, P.; Lohkamp, B.; Scott, W. G.; Cowtan, K., Features and development of Coot. *Acta Crystallogr. Sect. D. Biol. Crystallogr.* **2010,** *66* (4), 486-501.
51. Liebschner, D.; Afonine, P. V.; Baker, M. L.; Bunkóczi, G.; Chen, V. B.; Croll, T. I.; Hintze, B.; Hung, L.-W.; Jain, S.; McCoy, A. J., Macromolecular structure determination using X-rays, neutrons and electrons: recent developments in Phenix. *Acta Crystallographica Section D: Structural Biology* **2019,** *75* (10), 861–877.
52. Chen, V. B.; Arendall, W. B.; Headd, J. J.; Keedy, D. A.; Immormino, R. M.; Kapral, G. J.; Murray, L. W.; Richardson, J. S.; Richardson, D. C., MolProbity: all-atom structure validation for macromolecular crystallography. *Acta Crystallogr. Sect. D. Biol. Crystallogr.* **2010,** *66* (1), 12–21.
53. Kucukelbir, A.; Sigworth, F. J.; Tagare, H. D., Quantifying the local resolution of cryo-EM density maps. *Nat. Methods* **2014,** *11* (1), 63–65.
54. Goddard, T. D.; Huang, C. C.; Meng, E. C.; Pettersen, E. F.; Couch, G. S.; Morris, J. H.; Ferrin, T. E., UCSF ChimeraX: Meeting modern challenges in visualization and analysis. *Protein Sci.* **2018,** *27* (1), 14-25.
55. Raszewski, G.; Renger, T., Light Harvesting in Photosystem II Core Complexes Is Limited by the Transfer to the Trap: Can the Core Complex Turn into a Photoprotective Mode? *J. Am. Chem. Soc.* **2008,** *130* (13), 4431–4446.
56. Byrdin, M.; Jordan, P.; Krauss, N.; Fromme, P.; Stehlik, D.; Schlodder, E., Light harvesting in photosystem I: modeling based on the 2.5-Å structure of photosystem I from *Synechococcus elongatus*. *Biophys. J.* **2002,** *83* (1), 433–457.
57. Yin, S.; Dahlbom, M. G.; Canfield, P. J.; Hush, N. S.; Kobayashi, R.; Reimers, J. R., Assignment of the Qy absorption spectrum of photosystem-I from *Thermosynechococcus elongatus* based on CAM-B3LYP calculations at the PW91-optimized protein structure. *J. Phys. Chem. B* **2007,** *111* (33), 9923–9930.
58. Renger, T.; Schlodder, E., Modeling of optical spectra and light harvesting in photosystem I. In *Photosystem I. The Light-Driven Plastocyanin:Ferredoxin Oxidoreductase*, Golbeck, J. H., Ed. Springer: Dordrecht, 2006; Vol. 24, pp 595–610.
59. Renger, T.; Marcus, R., On the relation of protein dynamics and exciton relaxation in pigment–protein complexes: an estimation of the spectral density and a theory for the calculation of optical spectra. *J. Chem. Phys.* **2002,** *116* (22), 9997–10019.
60. Sumi, H., Theory on rates of excitation-energy transfer between molecular aggregates through distributed transition dipoles with application to the antenna system in bacterial photosynthesis. *J. Phys. Chem. B* **1999,** *103* (1), 252–260.
61. Scholes, G. D.; Fleming, G. R., On the mechanism of light harvesting in photosynthetic purple bacteria: B800 to B850 energy transfer. *J. Phys. Chem. B* **2000,** *104* (8), 1854–1868.
62. Jang, S.; Newton, M. D.; Silbey, R. J., Multichromophoric Förster resonance energy transfer. *Phys. Rev. Lett.* **2004,** *92* (21), 218301.
63. Wells, K. L.; Lambrev, P. H.; Zhang, Z. Y.; Garab, G.; Tan, H. S., Pathways of energy transfer in LHCII revealed by room-temperature 2D electronic spectroscopy. *Phys. Chem. Chem. Phys.* **2014,** *16* (23), 11640–11646.
64. Du, M.; Xie, X.; Jia, Y.; Mets, L.; Fleming, G. R., Direct observation of ultrafast energy transfer in PSI core antenna. *Chem. Phys. Lett.* **1993,** *201* (5–6), 535–542.
65. Yang, M.; Damjanović, A.; Vaswani, H. M.; Fleming, G. R., Energy transfer in photosystem I of cyanobacteria *Synechococcus elongatus*: model study with structure-based semi-empirical Hamiltonian and experimental spectral density. *Biophys. J.* **2003,** *85* (1), 140–158.
66. Melkozernov, A. N.; Lin, S.; Blankenship, R. E., Femtosecond transient spectroscopy and excitonic interactions in photosystem I. *J. Phys. Chem. B* **2000,** *104* (7), 1651–1656.
67. Rätsep, M.; Johnson, T. W.; Chitnis, P. R.; Small, G. J., The red-absorbing chlorophyll *a* antenna states of photosystem I: A hole-burning study of *Synechocystis* sp. PCC 6803 and its mutants. *J. Phys. Chem. B* **2000,** *104* (4), 836–847.
68. Croce, R.; Zucchelli, G.; Garlaschi, F. M.; Bassi, R.; Jennings, R. C., Excited state equilibration in the photosystem I−light-harvesting I complex: P700 is almost isoenergetic with its antenna. *Biochemistry* **1996,** *35* (26), 8572–8579.
69. Sener, M. K.; Lu, D.; Ritz, T.; Park, S.; Fromme, P.; Schulten, K., Robustness and optimality of light harvesting in cyanobacterial photosystem I. *J. Phys. Chem. B* **2002,** *106* (32), 7948–7960.
70. Damjanović, A.; Vaswani, H. M.; Fromme, P.; Fleming, G. R., Chlorophyll excitations in photosystem I of *Synechococcus elongatus*. *J. Phys. Chem. B* **2002,** *106* (39), 10251–10262.
71. Kramer, T.; Noack, M.; Reimers, J. R.; Reinefeld, A.; Rodríguez, M.; Yin, S., Energy flow in the Photosystem I supercomplex: Comparison of approximative theories with DM-HEOM. *Chem. Phys.* **2018,** *515*, 262–271.
72. Gobets, B.; Dekker, J.; van Grondelle, R., Transfer-to-the-trap limited model of energy transfer in Photosystem 1. In *Photosynthesis: mechanisms and effects*, Garab, G., Ed. Kluwer Academic: Dordrecht, the Netherlands, 1998; pp 503–508.
73. Scholes, G. D., Coherence from Light Harvesting to Chemistry. *J. Phys. Chem. Lett.* **2018,** *9* (7), 1568–1572.
74. Romero, E.; Augulis, R.; Novoderezhkin, V. I.; Ferretti, M.; Thieme, J.; Zigmantas, D.; Van Grondelle, R., Quantum coherence in photosynthesis for efficient solar-energy conversion. *Nature Physics* **2014,** *10* (9), 676–682.
75. Fuller, F. D.; Pan, J.; Gelzinis, A.; Butkus, V.; Senlik, S. S.; Wilcox, D. E.; Yocum, C. F.; Valkunas, L.; Abramavicius, D.; Ogilvie, J. P., Vibronic coherence in oxygenic photosynthesis. *Nat Chem* **2014,** *6* (8), 706–11.
76. Ma, F.; Romero, E.; Jones, M. R.; Novoderezhkin, V. I.; van Grondelle, R., Both electronic and vibrational coherences are involved in primary electron transfer in bacterial reaction center. *Nat. Commun.* **2019,** *10* (1), 933.

77. Tiwari, V.; Peters, W. K.; Jonas, D. M., Electronic resonance with anticorrelated pigment vibrations drives photosynthetic energy transfer outside the adiabatic framework. *Proc. Natl. Acad. Sci. U.S.A.* **2013,** *110* (4), 1203-1208.
78. Duan, H.-G.; Prokhorenko, V. I.; Cogdell, R. J.; Ashraf, K.; Stevens, A. L.; Thorwart, M.; Miller, R. J. D., Nature does not rely on long-lived electronic quantum coherence for photosynthetic energy transfer. *Proc. Natl. Acad. Sci. U.S.A.* **2017,** *114* (32), 8493-8498.
79. Butkus, V.; Zigmantas, D.; Valkunas, L.; Abramavicius, D., Vibrational vs. electronic coherences in 2D spectrum of molecular systems. *Chem. Phys. Lett.* **2012,** *545*, 40–43.
80. Rätsep, M.; Linnanto, J.; Freiberg, A., Mirror symmetry and vibrational structure in optical spectra of chlorophyll *a*. *J. Chem. Phys.* **2009,** *130* (19), 05B603.
81. Meneghin, E.; Pedron, D.; Collini, E., Raman and 2D electronic spectroscopies: A fruitful alliance for the investigation of ground and excited state vibrations in chlorophyll *a*. *Chem. Phys.* **2018,** *514*, 132–140.

TOC graphic